Fungal degradation strategies during solid-state fermentation of cereal brans with white-rot fungi

Bioresource Technology 461 (2026) 135424

Contents lists available at ScienceDirect

Bioresource Technology

journal homepage: www.elsevier.com/locate/biortech

Fungal degradation strategies during solid-state fermentation of cereal brans with white-rot fungi

Chloe Rantzos [a,b], Jorge Rencoret [c], José C. del Río [c], Amparo Jiménez-Quero [a,b,*]

[a] Division of Industrial Biotechnology, Department of LIFE Sciences, Chalmers University of Technology, Gothenburg, Sweden
[b] Wallenberg Wood Science Center, Department of LIFE Sciences, Chalmers University of Technology, Gothenburg, Sweden
[c] Instituto de Recursos Naturales y Agrobiología de Sevilla, CSIC, Avenida de la Reina Mercedes, 10, Seville 41012, Spain

HIGHLIGHTS

- Corn bran exhibited higher recalcitrance to fungal degradation than wheat bran.
- Fungal-degradation patterns showed dependence on substrate-species interactions.
- Early-stage metabolism preferentially targeted starch over structural carbohydrates.
- *Fomes fomentarius* resulted in the highest carbohydrate depletion in wheat bran.
- Fungal fermentation enriched corn bran in phenolics and altered their distribution.

GRAPHICAL ABSTRACT

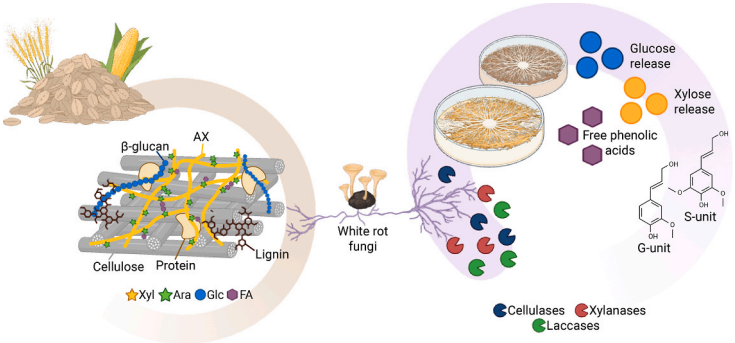

ARTICLE INFO

Keywords:
Lignocellulose degradation
Fungal pretreatment
Ferulic acid
Agricultural waste
Xylanases
Laccases

ABSTRACT

Cereal brans are abundant agro-industrial residues rich in polysaccharides, phenolic acids, and proteins, making them promising substrates for biotechnological valorization. This study investigated the progressive modification of wheat and corn bran during solid-state fermentation by three white-rot fungi (*Pleurotus ostreatus, Fomes fomentarius* and *Ganoderma lucidum*) to elucidate how fungal degradation performance is influenced by substrate composition. Fourier Transform Infrared Spectroscopy (FTIR) and Two-Dimensional Nuclear Magnetic Resonance (2D-NMR) analysis revealed preferential hemicelluloses degradation in both brans, accompanied by substantial alterations in signals associated with phenolic compounds, particularly ferulates. Among the tested fungi, *F. fomentarius* achieved the greatest carbohydrate reduction in wheat bran (51% w/w) and *P. ostreatus* in corn bran (15% w/w). All species degraded phenolic acids in wheat bran, while corn bran exhibited an enrichment of ferulic acid (up to 38% w/w), indicating greater structural recalcitrance. Enzymatic profiling showed that wheat bran promoted higher xylanase and cellulase activities, whereas laccase activity was primarily species-dependent. Overall, these findings provide a systematic understanding of fungal mediated degradation pathways in cereal brans and highlight the critical role of substrate composition in shaping white-rot fungi strategies in lignocellulosic bioprocesses.

* Corresponding author at: Chalmers University of Technology, The Dept. of Life Sciences (LIFE)Industrial Biotechnology, Kemivägen 10, Kurshus floor 6Gothenburg SE-412 96, Sweden.
E-mail address: amparo@chalmers.se (A. Jiménez-Quero).

https://doi.org/10.1016/j.biortech.2026.135424
Received 8 May 2026; Received in revised form 6 July 2026; Accepted 15 July 2026
Available online 17 July 2026

1. Introduction

Agricultural activities generate substantial amounts of lignocellulosic waste, with harvest residues from crops such as sugarcane, corn, rice, wheat, and palm oil having the largest contribution (Cazier et al., 2024). Among these, cereal grains -particularly wheat, corn and rice- are widely cultivated for global food production, with cereal bran constituting the primary side-stream of their processing. It is estimated that approximately 160 million tonnes of cereal bran are produced annually (Hadidi et al., 2024), highlighting its potential as an abundant and underutilized biomass resource.

Cereal byproducts are primarily composed of a lignocellulosic network, along with residual starch, water-soluble dietary fibers (mainly β-glucans), and proteins (Gari et al., 2024). In cell walls, cellulose and hemicelluloses are embedded within a lignin matrix, forming a complex and highly cross-linked architecture that differs with the plant species, stage of growth, and farming conditions (Sharma et al., 2019). Hemicelluloses are primarily arabinoxylans, with varying types and degree of substitutions that include α-L-arabinofuranosyl units, (4-*O*-methyl)-α-D-glucuronic acid, and *O*-acetyl groups (Van Eylen et al., 2011). Phenolic acids, such as ferulic and *p*-coumaric acids, are mostly esterified to the arabinofuranosyl residues and act as cross-links between the different polysaccharide chains, lignin, and proteins, contributing to the recalcitrance towards microbial and enzymatic degradation (Mnich et al., 2020). To facilitate recovery of sugars from lignocellulose, conventional pretreatment strategies in biorefinery schemes rely on chemical, physical, and physicochemical methods. Although effective, these approaches are usually associated with high energy requirements, the formation of inhibitory products, and limited selectivity (Sharma et al., 2025). Biological pretreatments, in contrast, offer milder processing conditions and greater substrate selectivity. However, their efficiency depends on the intricate interplay of variables and complex dynamics involved in fermentation and enzymatic processes (Sharma et al., 2019).

White-rot fungi (WRF) can produce a diverse array of enzymes that efficiently decompose lignocellulose (Andlar et al., 2018). Consequently, they represent a promising strategy for selective biological pretreatment, capable of altering both the chemical composition and structural integrity of the biomass on a macroscopic and microscopic level. Through solid-state fermentation (SSF), WRF can effectively degrade diverse cereal brans, demonstrating strong potential as a pretreatment for energy and materials applications (Sharma et al., 2025). For example, structural modifications induced by fungal growth have been shown to affect the performance of mycelium-based composite materials (Nejati et al., 2026). These effects highlight that the degradation efficiency and selectivity of WRF are strongly dependent on species-substrate interactions, underscoring the need for systematic studies of diverse residues using different fungal strains (Wu et al., 2019).

In this context, three fungal species, *Pleurotus ostreatus, Fomes fomentarius*, and *Ganoderma lucidum,* were investigated for their ability to degrade wheat and corn bran under SSF conditions. Fungal degradation was monitored by jointly assessing temporal changes in substrate composition and enzyme secretion profiles over 14 days. The solid fraction was thoroughly characterized in terms of monosaccharides composition, cellulose content, phenolic acid profiles, and lignin modifications, while crude extracts were evaluated for activities of cellulases, xylanases and laccases. By correlating secreted enzyme dynamics with compositional and structural alterations, this study aims to elucidate degradation patterns and clarify substrate-fungus interactions in small-scale SSF conditions, providing mechanistic insights into biological pretreatment processes relevant to cereal bran valorization.

2. Materials and methods

2.1. Substrate materials and fungal cultures

Wheat bran (WB) and corn bran (CB) were kindly provided by Lantmännen Cerealia AB, Nord Mills (Sweden) and Extractis (France), respectively. Substrates had an average particle size of 3 mm and were dried at 40 °C for 24 h before storing them in the darkness in a dry and cool room (21 °C) until their use.

P. ostreatus, F. fomentarius (DSM 3520), and *G. lucidum* were obtained from Svamphuset (Sweden) and from Deutsche Sammlung von Mikroorganismen und Zelhulturen (DSMZ, Germany). The cultures were maintained on potato dextrose agar plates and were subcultured every 1 week.

All chemicals, standards and reagents were of analytical grade and obtained from Sigma-Aldrich (Sweden), unless otherwise mentioned.

2.2. Inoculum preparation and solid-state fermentation of wheat and corn bran

Fermentation experiments were conducted in triplicate for each fungal strain using both wheat and corn bran as substrates. The brans were sterilized by autoclaving at dry conditions at 121 °C for 20 min (Tuttnauer, Sweden). Prior to inoculation, pre-cultures were prepared for each substrate-fungus combination by adding PDB to 10 g of bran at 70% moisture content, along with a 6 mm mycelial agar plug from a 7-day old culture. Cultures were incubated at 30 °C for 7–10 days until full colonization was achieved, with mixing every two days to ensure uniform growth.

The experimental set up consisted of static cultures in Petri dishes (90 mm) using WB and CB as the main macronutrients source. In each petri dish, 5 g of dry substrate, adjusted to 70% moisture content with water, were inoculated with 10 wt% of the pre-culture and mixed thoroughly. Plates were incubated in the darkness at 30 °C for 3, 5, 7, 10 and 14 days. Non inoculated plates were kept at the same conditions and used as control samples.

2.3. Crude extracts recovery and solid fraction separation

At each time point, half of the solids were mixed with 25 mL of 0.05 M pH 5 citrate buffer to recover the secreted fungal enzymes. The suspensions were incubated at 30 °C and 300 rpm for 1 h, then centrifuged at 4700 g for 15 min, before filtering the supernatant through 0.45 µm Nylon filters. The solids were washed twice with MilliQ water before freeze-drying and analyzing their compositional changes.

The remaining half of the plate was dried at 55 °C for 48 h and used for the NMR analysis.

2.4. Determination of fungal biomass

To determine fungal biomass in the solids, ergosterol was extracted and quantified according to the method by (Rubio-Ríos et al., 2021). Samples were analyzed in a high-pressure liquid chromatography system (Vanquish Core, Thermo Fischer Scientific, USA) using a Luna 5 µm C18 100 Å LC column (250 x 4.6 mm, Phenomenex, USA) connected to a DAD detector (Vanquish Core, Thermo Fischer Scientific, USA). For each fungal species, a standard curve relating fungal biomass to ergosterol content was established.

2.5. Compositional analysis of solids

Cellulose, hemicelluloses and lignin in the two brans and fermented solids were analyzed using an adaptation of the National Renewable Energy Laboratory (NREL) protocol for the determination of structural carbohydrates and lignin in biomass (NREL-TP-510-42618) in combination with trifluoracetic acid (TFA) hydrolysis for the estimation of the

non-crystalline sugars (hemicelluloses), following the method of (Pereira and Jiménez-Quero, 2025). Cellulose was measured as the difference of glucose after sulfuric acid hydrolysis and glucose after TFA hydrolysis. Arabinoxylan content was calculated as the total arabinose and xylose, while β-D-glucan content was determined by subtracting starch from the glucose determined after sulfuric hydrolysis. Quantification of monosaccharides was performed using high performance anion-exchange chromatography with pulsed amperometric detection (HPAEC-PAD) (Dionex ICS-6000, Thermo Fischer, USA). The analysis was executed using a Dionex CarboPac PA20 column (3 × 150 mm, Thermo Fischer Scientific). Separation of neutral sugars was achieved according to (Qazanfarzadeh et al., 2026).

Acid insoluble lignin was calculated gravimetrically after sulfuric acid hydrolysis and drying at 105 °C for 24 h (SENTRY Xpress4.0, Paragon, USA).

Acid soluble lignin was estimated by UV–Vis spectrometry of the filtered sulfuric acid hydrolysates at 320 nm (PV4 Visible Spectrophotometer, VWR, Sweden)($\varepsilon_{320} = 30\ Lg^{-1}cm^{-1}$).

Ash content was determined gravimetrically after heating at 550 °C for 24 h (SENTRY Xpress4.0, Paragon, USA), while moisture content was estimated gravimetrically (Touch moisture analyzer, VWR, Sweden).

Total starch content was determined spectrophotometrically at 510 nm against a glucose standard curve, according to the Total Starch kit by Megazyme (Megazyme, Ireland).

Total protein content was estimated by total nitrogen concentration (rapid MAX N exceed, elementar, Sweden) using a protein factor equal to 5.6 (Medina-Remón et al., 2009).

Total phenolics were determined by saponification of the biomass followed by high-performance liquid chromatography (HPLC). Solids were subjected to saponification with 2 M NaOH at 80 °C under stirring overnight. Saponified samples were acidified to pH 2 with 12 M HCl, and phenolics were extracted by partition with ethyl acetate (1:6, v/v). The ethyl acetate fractions were then dried under N_2 and resuspended in methanol:0.1% formic acid (1:1, v/v). Samples were analyzed in a Luna 3 μm C18 100 Å LC column (150 × 4.6 mm, Phenomenex, USA) using a DAD detector (Vanquish Core, Thermo Fischer Scientific, USA) according to the method described in (Pereira and Jiménez-Quero, 2025).

2.6. Determination of solubilized sugars and phenolics in the crude extracts

Reducing sugars were measured spectrophotometrically with the DNS method at 540 nm adapted to a 96-well plate according to (Gonçalves et al., 2010). Calibration curves of glucose and/or xylose were used to determine the concentration of reducing sugars.

Free phenolics in the extracts were measured spectrophotometrically with the Folin-Ciocalteu (FC) method at 760 nm adapted to a 96-well plate (Cicco et al., 2009). Ferulic acid was used as standard, and results were expressed as ferulic acid equivalents (FAE).

2.7. Fourier Transform Infrared Spectroscopy (FTIR) analysis

The chemical structures of the solids were characterized by Attenuated Total Reflectance Fourier Transform Infrared Spectroscopy (ATR-FTIR). Milled samples were scanned in ambient conditions on a PerkinElmer Spectrum 3 FTIR spectrometer equipped with a GladiATR accessory (PIKE Technologies, USA). The MIR range was from 4000 cm^{-1} to 400 cm^{-1} at a spectral resolution of 4 cm^{-1} with an accumulation of 32 scans.

2.8. Two-Dimensional Nuclear Magnetic Resonance (2D-NMR) analysis

Raw substrate, used as control, and the last day of fermentation (14-day) were analyzed directly by 2D-NMR at the gel state following the method previously described (Kim et al., 2008; Rencoret et al., 2009). Approximately 60 mg of finely ball-milled material were swollen in 0.6 mL of DMSO-d_6. Two-dimensional Heteronuclear Single Quantum Coherence (2D-HSQC) NMR spectra were acquired at 300 K using a Bruker AVANCE III 500 MHz spectrometer equipped with a 5 mm cryogenically cooled TCI inverse-geometry gradient probe (Bruker, Germany). Experiments were performed using the standard Bruker pulse sequence "hsqcetgpsisp2.2". The spectra were acquired from 10 to 0 ppm in F2 (^{1}H) using 1000 data points (TD) for an acquisition time of 100 ms and from 200 to 0 ppm in F1 (^{13}C) using 256 increments of 32 scan for a total experiment time of 2 h 34 min. A one-bond $^1J_{CH}$ coupling constant of 145 Hz was applied. Data processing used typical matched Gaussian apodization in F2 (LB = −0.1, GB = 0.001) and a squared cosine bell in F1 (LB = 0.3, GB = 0.1). Chemical shifts were referenced to the central DMSO solvent signal (δ_C/δ_H = 39.5/2.49 ppm) and the spectra were normalized to the same DMSO signal intensity to allow comparison among samples, as identical sample masses and solvent volumes were used. HSQC signal assignments were performed by comparison with literature data (Kim et al., 2017; Ruthes et al., 2020; Smiderle et al., 2010; del Río et al., 2018). A semiquantitative analysis of HSQC cross-peaks was conducted by volume integration using Bruker TopSpin 4.2 software. Relative abundances of carbohydrate components were estimated from the volume integrals of the anomeric correlation signals corresponding to arabinose, α-glucans, and sucrose. For lignin and associated phenolic compounds, including hydroxycinnamic acids (SA, FA, and *p*CA) and diferuloylputrescine (dFP), relative contents were calculated from the integrals of characteristic correlations: G_2 and $S_{2,6}$ for lignin units; $SA_{2,6}$, FA_2, $pCA_{2,6}$, and dFP_7 for the phenolic components. The volume integrals of those correlation signals involving two proton-carbon pairs ($S_{2,6}$, $SA_{2,6}$, and $pCA_{2,6}$) were halved.

2.9. Enzyme activities

The crude extracts at each time point were analyzed to determine the enzymatic activities of Laccases, Cellulases and Xylanases.

Laccase (Lac) activity was measured following the oxidation of 2,2′-azino-bis(3-ethylbenzothiazoline-6-sulfonic acid) (ABTS) method (More et al., 2011). Specifically, Lac was assayed in a 96-well plate system containing 100 μL of 100 mM pH 5 sodium acetate and 100 μL of 0.5 mM ABTS solution with the addition of 50 μL of suitably diluted crude enzyme extract. The plate was incubated for 5 min at room temperature while measuring the change in the absorbance. Oxidation of ABTS was monitored by determining the increase in A_{420} ($\varepsilon_{420} = 3.6 \times 10^4\ M^{-1}cm^{-1}$) and one unit of enzyme activity was defined as the amount of enzyme needed to oxidize 1 μmol of ABTS per minute.

Cellulases (*endo*-1,4-β-D-glucanase) were assayed in a system containing AZO-Barley Glucan (Megazyme, Ireland) at 40 °C for 10 min under stirring, according to the manufacturer's protocol. The activity of the samples was calculated by reference to a standard curve of *endo*-1,4-β-D-glucanase (Megazyme, Ireland). One unit of enzyme activity was defined as the amount of enzyme required to release 1 μmol of glucose from barley glucan in 1 min at the specified assay conditions.

The total activities of xylanases were measured using as substrate 1% w/v beechwood xylan (Megazyme, Ireland) dissolved in 0.05 M pH 5.3 Na-citrate buffer at 50 °C for 5 min, according to the method of (Bailey et al., 1992). The reaction was terminated by transferring 25 μL of the mixture in a 96-well plate containing DNS and measuring the reducing sugars over a xylanase standard curve as described in section 2.6.

2.10. Statistical analysis

All data are expressed as mean ± standard deviation. A one-way Analysis of Variance (ANOVA) was used to assess statistical significance at a 5% level for measurements performed only on the last day of fermentation (day 14), while a two-way ANOVA was implemented on samples from different fermentation time points (days 3, 5, 7, 10, 14). All samples were in biological triplicates. Control was included as a reference group and significant differences among groups means were

further evaluated with Tukey HD test.

3. Results and Discussion

3.1. Compositional characterization of wheat and corn bran

To establish a baseline for interpreting fungal degradation behavior, the chemical compositions of wheat bran (WB) and corn bran (CB) were first characterized. In the present study, both substrates were used as the main nutrient sources during solid-state fermentation (SSF) with *P. ostreatus, F. fomentarius* and *G. lucidum*. Their initial compositional profiles, summarized in Table 1, provided the reference framework for evaluating any subsequent biochemical transformation.

Both residues showed high carbohydrates contents, reaching 593.1 ± 31.6 mg g_{DW}^{-1} in WB and 743.7 ± 19.8 mg g_{DW}^{-1} in CB, while their lignin contents were relatively low (114.6 ± 0.9 mg in WB, and 89.0 ± 3.0 mg g_{DW}^{-1} in CB). The carbohydrate fraction was rich in glucose, present as α-glucans in starch, β-glucan fibers, and cellulose. In accordance with previous studies, the main hemicellulose components were arabinoxylans, accounting for 264.7 ± 7.4 mg g_{DW}^{-1} in WB and 336.3 ± 10.4 mg g_{DW}^{-1} in CB (Roye et al., 2020). Minor amounts of other cell wall monosaccharides, including galactose and mannose, were also detected.

Phenolic acids are considered among the major groups of bioactive compounds in cereal biomass. The total concentration of phenolics was higher in CB (78.8 ± 2.0 mg g_{DW}^{-1}) than in WB (16.8 ± 4.5 mg g_{DW}^{-1}). Ferulic acid was the predominant phenolic acid in both brans, while sinapic acid was also present in substantial amounts in WB.

Other differences lied in the protein content, where WB exceeded CB by threefold and in ash content.

Table 1
Total chemical composition of Wheat bran and Corn bran.

	Wheat bran	Corn bran
Moisture (%)	8.0 ± 0.2	10.0 ± 0.1
Carbohydrate content (mg g_{DW}^{-1})[a]	593.1 ± 31.6	743.7 ± 19.8
Rha (% total sugars)	0.0 ± 0.0	0.0 ± 0.0
Ara (% total sugars)	15.4 ± 0.2	15.6 ± 0.1
Gal (% total sugars)	2.2 ± 0.2	6.1 ± 0.1
Glc (% total sugars)	53.2 ± 0.3	47.9 ± 0.2
Xyl (% total sugars)	29.2 ± 0.2	29.6 ± 0.2
Man (% total sugars)	0.0 ± 0.0	0.8 ± 0.1
AX (mg g_{DW}^{-1})[b]	264.7 ± 7.4	336.3 ± 10.4
Starch (mg g_{DW}^{-1})	148.3 ± 24.5	182.3 ± 1.9
β-D-glucans (mg g_{DW}^{-1})[c]	167.4 ± 29.5	174.0 ± 14.2
Protein content (mg g_{DW}^{-1})	157.4 ± 2.4	58.1 ± 3.2
Total phenolics (mg g_{DW}^{-1})[d]	16.8 ± 4.5	78.8 ± 2.0
Gentisic acid (% total phenolics)	10.4 ± 1.2	4.2 ± 0.5
Catechin (% total phenolics)	0.0 ± 0.0	2.0 ± 0.2
Vanillic acid (% total phenolics)	1.4 ± 0.2	1.4 ± 0.2
Caffeic acid (% total phenolics)	7.0 ± 0.6	5.8 ± 0.1
p-coumaric acid (% total phenolics)	1.0 ± 0.1	7.4 ± 0.2
trans-ferulic acid (% total phenolics)	52.1 ± 3.3	69.5 ± 0.6
Sinapic acid (% total phenolics)	31.4 ± 2.1	7.0 ± 0.3
trans-cinnamic acid (% total phenolics)	0.5 ± 0.1	2.7 ± 0.1
Cellulose (% DW)	14.1 ± 3.2	20.1 ± 3.2
Hemicelluloses (% DW)	45.2 ± 1.1	54.3 ± 1.3
Acid soluble lignin (% DW)	0.0 ± 0.0	0.0 ± 0.0
Acid insoluble lignin (% DW)	11.5 ± 0.1	8.9 ± 0.3
Ash content (% DW)	6.5 ± 0.1	1.2 ± 0.0

[a] DW: dry-weight basis. Carbohydrate content determined as the sum of monosaccharides determined after H_2SO_4 hydrolysis and HPAEC-PAD analysis.
[b] Arabinoxylan (AX) content calculated as the total arabinose (Ara) and xylose (Xyl) composition.
[c] β-D-glucan content determined by subtracting starch from total glucose content, as determined after H_2SO_4 hydrolysis and HPAEC-PAD analysis.
[d] Total phenolics determined as the sum of phenolic acids determined after NaOH saponification and HPLC analysis.

3.2. Fungal colonization and growth

Solid-state fermentation of WB and CB was carried out over a 14-day period to evaluate the ability of *P. ostreatus*, *F. fomentarius* and *G. lucidum* to colonize the lignocellulosic material. All three fungi showed active growth already from day 3, with WB exhibiting a faster colonization rate as shown in Fig. 1a and 1b.

Ergosterol content was used as a quantitative indicator of fungal growth. Ergosterol is the primary sterol in the cell membranes of filamentous fungi and can be a minor component in higher plants (Pasanen et al., 1999). No ergosterol was detected in the WB and CB controls. After growth on potato dextrose broth, *P. ostreatus*, *F. fomentarius*, and *G. lucidum* mycelia contained 2.3 ± 0.2, 1.8 ± 0.2, and 3.0 ± 0.3 $mg_{ergosterol}/g_{dry\ mycelium}$, respectively.

Overall, WB samples exhibited a higher ergosterol content indicating more advanced colonization (Fig. 1c). In both substrates, *F. fomentarius* had a steady growth rate until day 7 before stabilizing in CB or dropping in WB, possibly reflecting the transition towards a late-stage mycelial growth. *G. lucidum* increased rapidly in WB without reaching the lag phase in 14 days, whereas *P. ostreatus* remained relatively stable in WB and showed a small increase in CB. All species demonstrated faster fungal growth in the early days of the fermentation when easily accessible nutrients like starch were more available.

3.3. Compositional changes during solid-state fermentation

Solid-state fermentation (SSF) with white-rot fungi is a dynamic process in which substrate depletion through fungal metabolism is accompanied by mycelium growth and secondary metabolites production. Fungal mycelium is composed primarily of β-glucans, proteins and chitin (Gow et al., 2017), all of which can influence the final composition of the resulting solids. The sequential substrate degradation, nutrient release and uptake are both species and substrate dependent, highlighting the need for system specific evaluation prior to biorefinery integration. In the present study, the bran substrates were the main source of macronutrients. As shown in Table 1, starch, β-D-glucans and arabinoxylans (AX) were the dominant polysaccharides in both brans. To determine the evolution of the carbohydrates profile throughout the fermentation period, monosaccharides analysis of the solids and quantification of the released sugars in the extracts were performed. It should be noted that, following harvest, solids were distributed for different analytical purposes, precluding mass balance tracking and, thus, limiting determination of absolute changes in the composition of the solids.

Autoclaving and extraction steps influenced the carbohydrate composition of the substrates, therefore all comparisons were made relative to the control samples (Table S1).

All species decreased the concentration of total carbohydrates in WB after 14 days, with *F. fomentarius* exhibiting the greatest effect (Fig. 2a). *G. lucidum* caused an initial increase in days 3 and 5, mostly in arabinose and β-glucan content (Table S1). In contrast, *P. ostreatus* reduced total carbohydrates by day 3, after which levels remained relatively stable. Among the different components, starch displayed the highest relative decrease in all species, indicating its preferred consumption over AX and β-glucans. Starch is an excellent energy source as it is mostly soluble and the hydrolysis of its α-bonds leads to the release of small sugar units, such as maltose and glucose, making its breakdown a priority for fungal growth (Castorina et al., 2023). AX concentration slightly decreased by day 3 with *P.ostreatus* and *G. lucidum*, then remained stable. In contrast, *F. fomentarius* induced a stronger effect leading to 67% reduction by day 14. Concentration of β-glucans decreased the most after fermentation with *F. fomentarius* (49%), followed closely by *P. ostreatus* (44%). *G. lucidum* displayed a fluctuating trend in β-glucans concentration, with an 82% reduction by day 10 before exceeding control levels by day 14. This behavior may be explained by the concurrent substantial decrease in starch content during the same period, together with an increase in

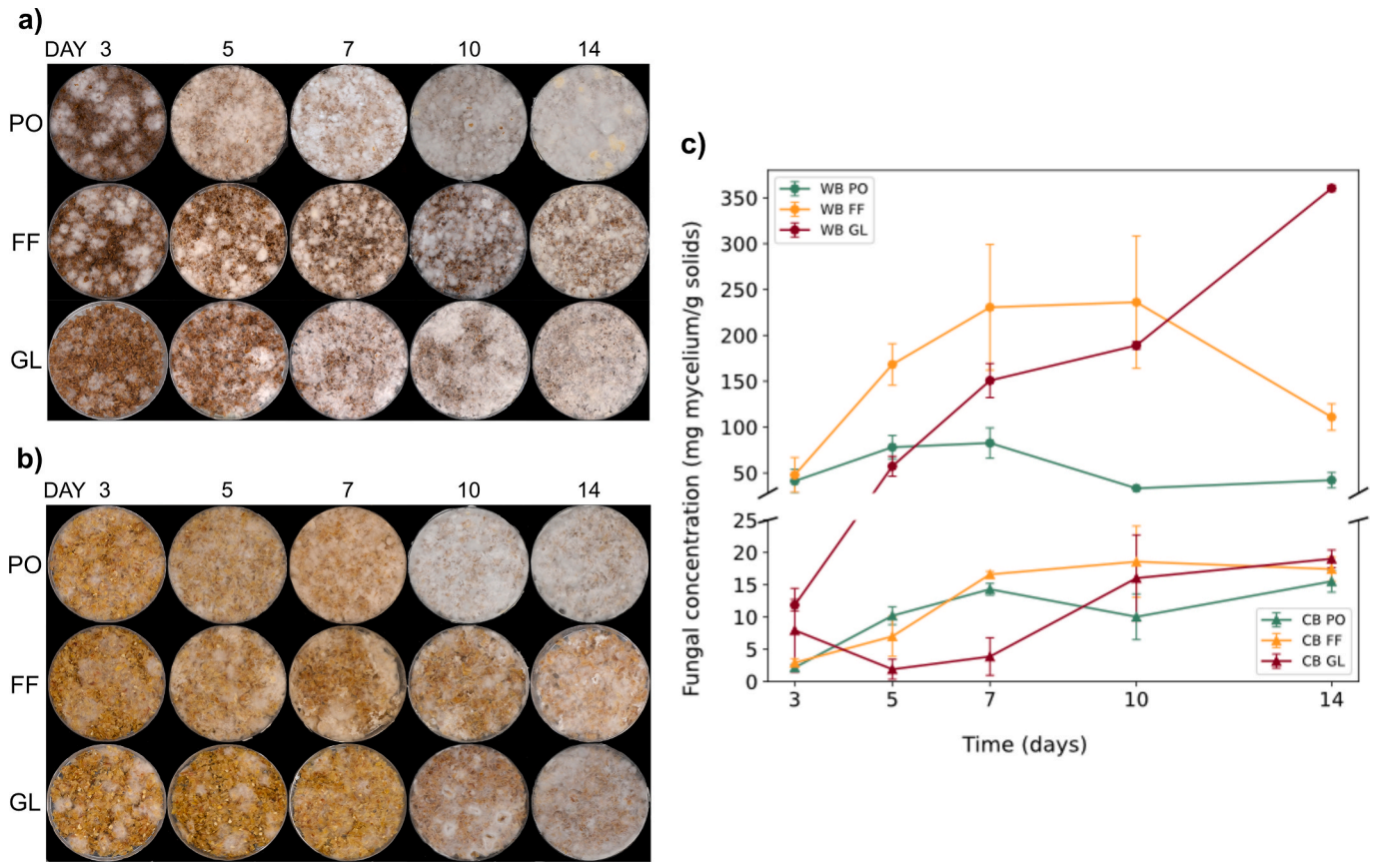

Fig. 1. Fungal growth during the solid-state fermentation of wheat bran (WB) and corn bran (CB). Colonized plates of (a) WB and (b) CB after 3, 5, 7, 10, 14 days of SSF with *P. ostreatus* (PO), *F. fomentarius* (FF) and *G. lucidum* (GL). (c) Fungal concentration in the solids ($mg_{mycelium}/g_{solids}$) measured based on their ergosterol content. Data represent mean ± SD (n = 3 biological replicates).

fungal biomass (Fig. 1c), which is largely composed of β-glucans (Gow et al., 2017).

Similarly, changes in the total carbohydrates of CB (Fig. 2c) showed that *P. ostreatus* was the only species inducing a reduction (15%), while *F. fomentarius* and *G. lucidum* caused no significant depletion. All species exhibited enrichment in β-glucans in conjunction with starch consumption to approximately 50% of its initial concentration.

Glucose and xylose release profiles during the fermentation (Fig. 2b, 2d) peaked on day 3 for WB and day 7 for CB before stabilizing at lower concentrations by day 14. The delayed sugar release observed in CB reflects its higher recalcitrance compared to WB, due to its less accessible structure with higher cellulose and AX content (Fig. 2e) (Roye et al., 2020).

In both bran fermentations, *P. ostreatus* displayed a preferential degradation of hemicelluloses and other amorphous carbohydrates over crystalline cellulose (Fig. 2a, 2c, 2e). In WB, *F. fomentarius* caused a 43% reduction in cellulose concentration, *G. lucidum* led to a 56% increase, and *P. ostreatus* had no significant effect. In contrast, cellulose concentration in CB increased after treatment with both *F. fomentarius* (28%) and *G. lucidum* (27%), whereas *P. ostreatus* resulted in a 10% decrease. Interestingly, the carbohydrate degradation strategy of *F. fomentarius* appeared substrate-dependent, with a pronounced reduction in both total carbohydrates and cellulose in WB, but with a very moderate effect on CB. Discrepancies in cellulose degradation by *F. fomentarius* depending on the wood substrate have also been previously reported by (Wei et al., 2024).

Protein levels increased by the end of fermentation (Fig. 2f), likely reflecting the continuous synthesis of protein during mycelium growth (Weng et al., 2025), as well as a relative increase due to the degradation of other fractions. All WB fermentations resulted in a significant increase in the protein content, while CB solids displayed less extensive changes. Protein content was estimated from total nitrogen in the solid fraction, which includes substrate and mycelium proteins, but also *N*-containing chitin and chitosan from the fungal cell wall (*N*-acetylglucosamine, glucosamine) (Castorina et al., 2023).

Those results are further supported by the change in relevant peaks of the FTIR spectra, especially in the bands corresponding to the stretching of the functional groups in lignocellulosic tissues (Fig. S1) and the contributions from the mycelium (Fig. S2). Fungal fermentation induced a noticeable reduction in the absorbance at 1730 cm^{-1}, attributed to the carbonyl stretching of ester bonds in hemicelluloses (acetyl and ferulate groups) (Akbari et al., 2023). Additionally, the peak between 1200–1230 cm^{-1} corresponding to the stretching vibration of the C-O-C linkages in ethers and esters of phenolic hydroxyls (Shankar et al., 2022) demonstrated a slight change in the absorbance of the fermented samples, indicating the modification of the phenolic acids in the cereal cell wall.

To further explore this, the phenolic compounds present in the brans were extracted in two time points, halfway through and in the end of the fermentations. Control samples showed a lower total concentration than the original substrates, while maintaining the same ratio among phenolics (Fig. 3a, 3b, detailed in Table S2). Wheat bran contained high levels of ferulic and sinapic acids, whereas corn bran was rich in ferulic and *p*-coumaric acids.

In cereal biomass, phenolics include phenolic acids, flavonoids (e.g. catechin) and other compounds primarily in the bound form as conjugates with sugars, fatty acids or protein (Kähkönen et al., 1999). Fungal species adapted differently to that fraction of the biomass, validating the relative recalcitrance of CB as also indicated by the ergosterol content measurements in Fig. 1c. Growth of basidiomycetes in different

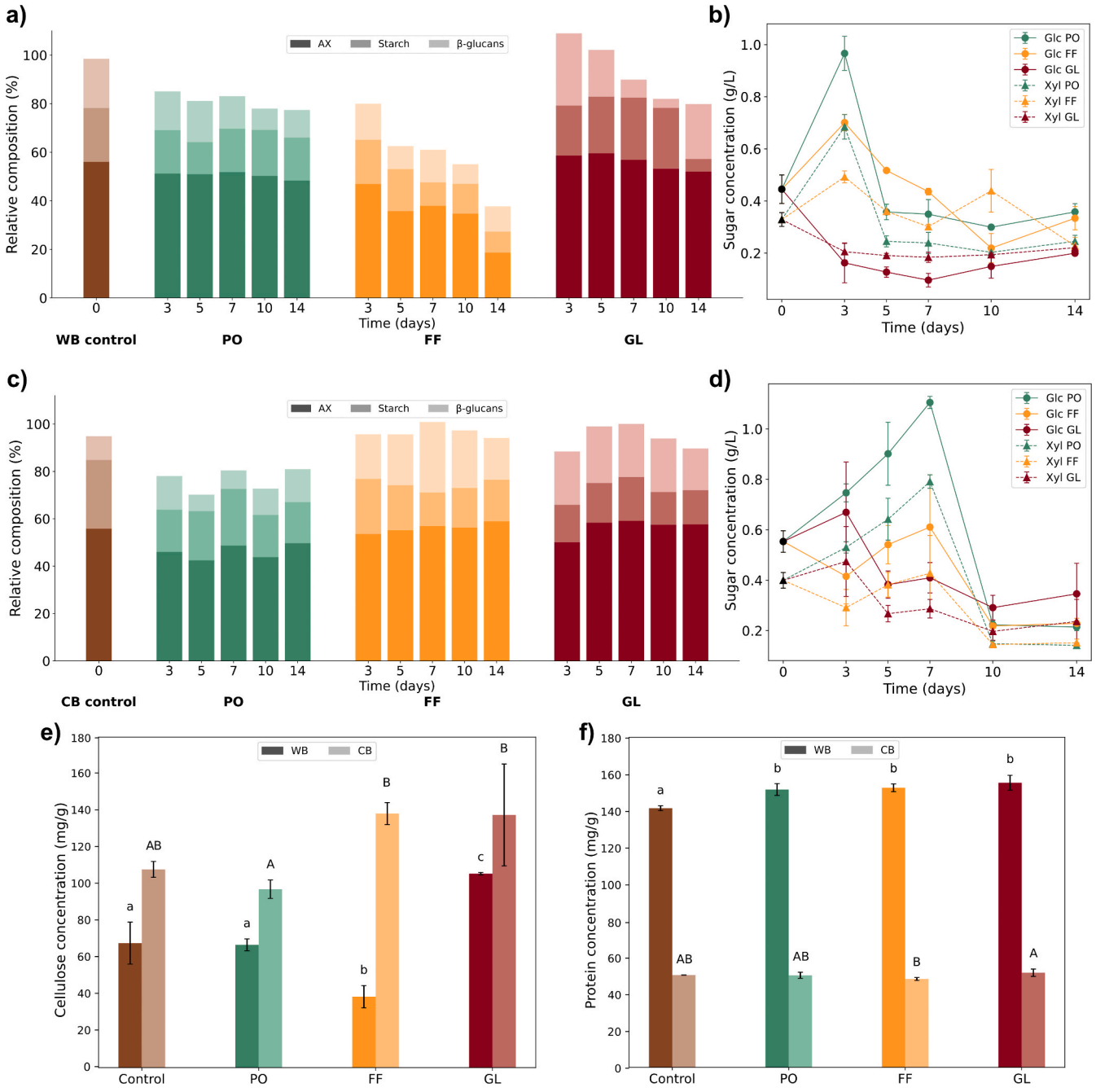

Fig. 2. Evolution of starch, β-glucans, arabinoxylans (AX) composition and released glucose (Glc) and xylose (Xyl) in (a), (b) wheat bran (WB) and (c), (d) corn bran (CB) after 3, 5, 7, 10 and 14 days of solid-state fermentation with *P. ostreatus* (PO), *F. fomentarius* (FF) and *G. lucidum* (GL). Dark shades correspond to the AX component, moderate shades to the β-glucan component and light shades to the starch component for each species. (e) Cellulose concentration (mg/g) and (f) Protein content (mg/g) in control samples and in fermented samples after 14 days. Dark shades correspond to WB as a substrate whereas the lighter shades correspond to CB. Bars represent the means ± SD (n = 3 biological replicates). Within the same variables, the lowercase letters (a-c) indicate significant differences among the values for WB, and the uppercase letters (A-B) for CB ($p < 0.05$).

substrates through SSF has been associated with phenolic compounds consumption and production through their secondary metabolism or enzymatic processes (Mäkelä et al., 2015).

Phenolic acids in WB were progressively degraded by all fungal species over the course of the fermentation. Ferulic acid concentration exhibited the greatest reduction across all species, followed by sinapic acid. After 14 days, *P. ostreatus, F. fomentarius*, and *G. lucidum* reduced total phenolics by 61%, 57% and 13%, respectively. *G. lucidum* additionally displayed a 305% increase in the content of free phenolic acids released in the extracts after 14 days of fermentation (Fig. 3c), the highest among all species. These results align with (Weng et al., 2025), where a 427% increase in free phenolic content was reported after 53 days of fermentation. *P. ostreatus* and *F. fomentarius* had no significant effect on the concentration of the phenolics released ($p>0.05$), possibly implying immediate uptake after cleaving from the solids as reported in previous studies (Goudopoulou et al., 2010; Heidari et al., 2022).

CB solids, by contrast, became enriched in total phenolic acids, while the relative proportions of individual compounds remained constant throughout fermentation (Table S2). After 14 days, all fermented samples showed an increase in phenolic acid content, which may reflect

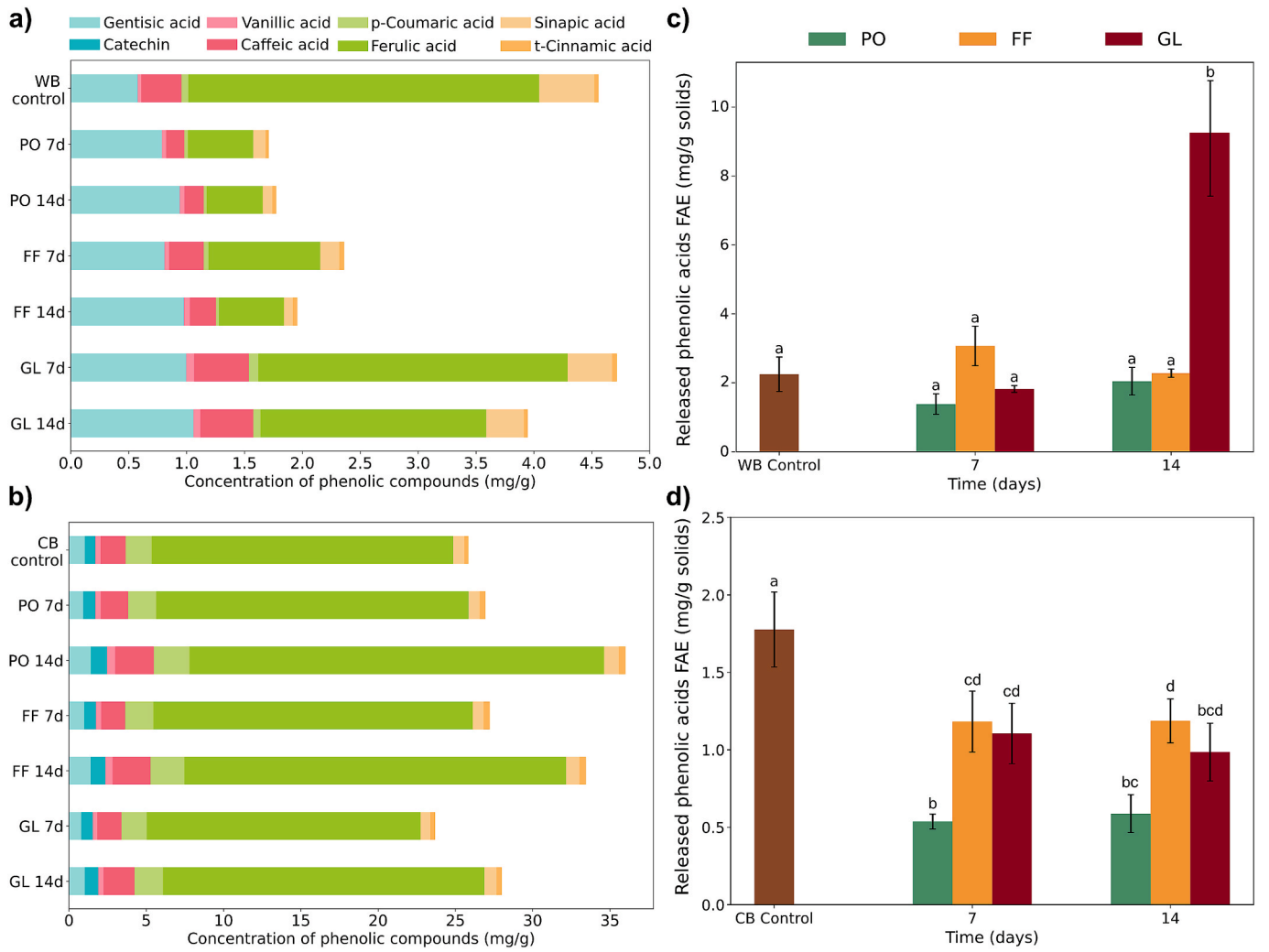

Fig. 3. Concentration of total phenolics (mg/g solids) in (a), (c) wheat bran (WB) and (b), (d) corn bran (CB) solids and released in extracts, respectively, after 7 and 14 days of solid-state fermentation with *P. ostreatus* (PO), *F. fomentarius* (FF) and *G. lucidum* (GL). Bars represent the means ± SD (n = 3 biological replicates). The lowercase letters (a-d) indicate significant differences among the values reported for each substrate ($p < 0.05$).

enhanced accessibility to alkali extraction following fungal modification of the cell wall (Šelo et al., 2024), the transient accumulation of degradation intermidates (Saharan et al., 2017), and/or the greater recalcitrance of the phenolic fraction relative to carbohydrates. In contrast, free phenolic acids in the extracts decreased significantly during fermentation (Fig. 3d), suggesting their preferential consumption by the fungi before the more recalcitrant bound phenolics (Castaño et al., 2022).

The high ergosterol content in *G. lucidum* fermented WB (Fig. 1c) sustained alongside a significant accumulation of released phenolics (Fig. 3c), indicated that *G. lucidum* was not inhibited by the elevated phenolic environment but rather continued to grow actively. This is consistent with the observations by (Castorina et al., 2023), where *G. annularis* displayed advanced growth rates and phenolics utilization relative to *P. ostreatus* when grown on corncobs.

3.4. Structural modifications of WB and CB components after SSF

The structural modifications of the different components, namely phenolic acids, lignin, and hemicelluloses in wheat bran (WB) and corn bran (CB) after 14 days of fermentation with *F. fomentarius*, *P. ostreatus*, and *G. lucidum* were investigated by 2D-HSQC-NMR spectroscopy. The 2D-HSQC-NMR spectra, showing the aromatic/unsaturated (δ_C/δ_H 100–150/6.0–8.0) and anomeric regions (δ_C/δ_H = 90–110/3.8–5.5), are shown in Fig. 4 (for WB samples) and Fig. 5 (for CB samples). The spectra revealed signals corresponding to lignin units, phenolic acids, proteins, and carbohydrates. The volume integrals of the characteristic signals for the different phenolic acids, lignin units, and carbohydrates, relative to the residual DMSO signal and corrected for sample weight, are summarized in Table 2, enabling direct comparison among samples derived from the same substrate.

The spectrum of the WB control sample was dominated by ferulate (FA), sinapate (SA), and protein-derived aromatic signals, with minor syringyl (S) and guaiacyl (G) lignin units signals, the later visible only after increasing the spectral intensities. Following fermentations, SA signals were undetectable in all fermented samples, while FA signals were entirely eliminated by *F. fomentarius* and *P. ostreatus,* with only minor amounts remaining after treatment with *G. lucidum*. Lignin-derived signals were similarly reduced, most strongly with *F. fomentarius*, followed by *G. lucidum* and, to a lesser extent, *P. ostreatus* (Table 2). S-type lignin was preferentially targeted over G-type lignin, likely due to structural differences between the two types. S-lignin is rich in β–*O*–4 alkyl-aryl ether linkages, which are relatively labile and more accessible to oxidative and enzymatic cleavage, while G-lignin contains more condensed, recalcitrant linkages, such as β–5 and 5–5 bonds, which are more resistant to depolymerization (Martínez et al., 2005; van Erven et al., 2018). The parallel reduction of FA, SA, and lignin signals in *F. fomentarius* fermented samples suggests degradation of lignin-

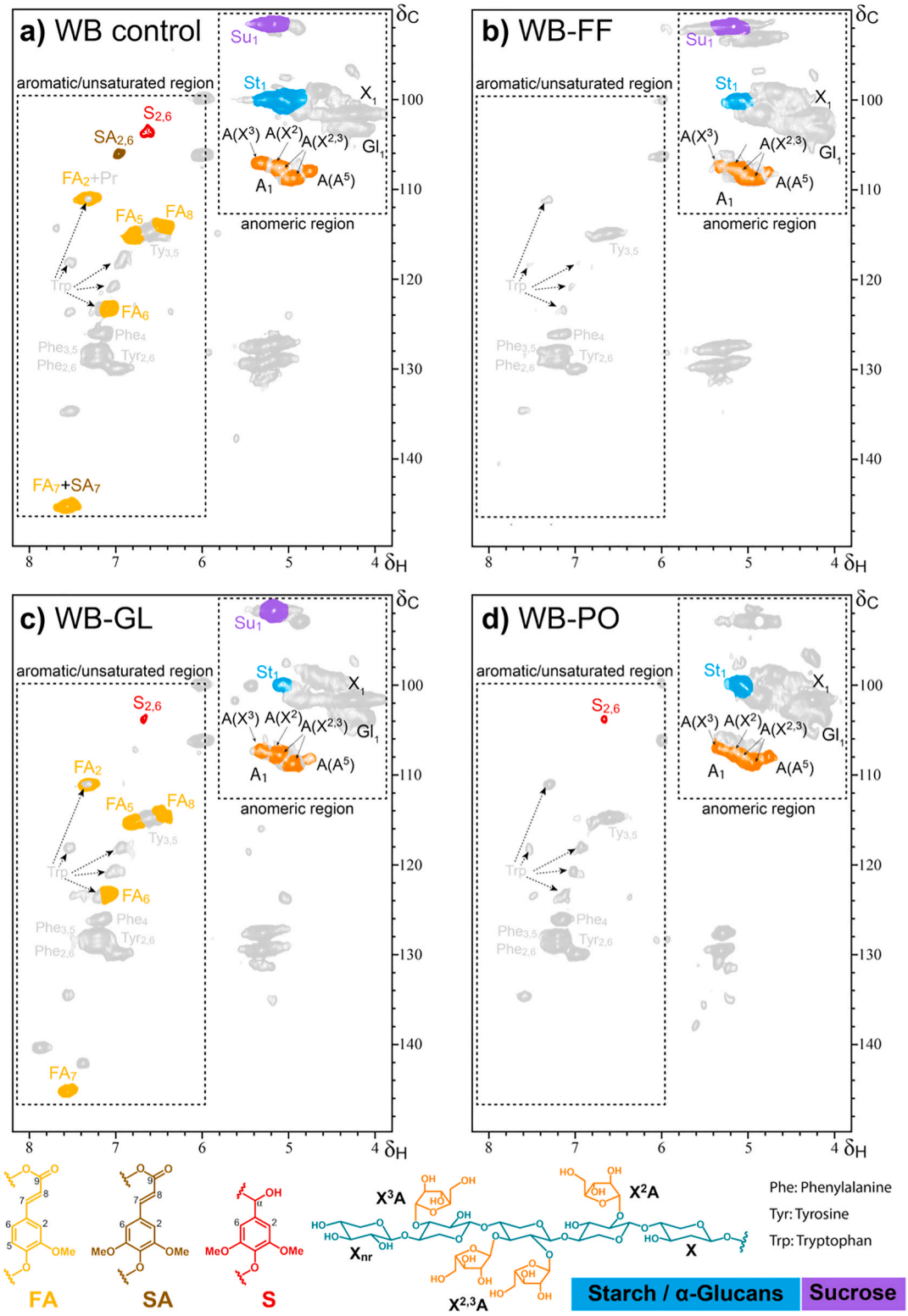

Fig. 4. 2D-HSQC spectra (δ_C/δ_H = 90–150/3.8–8.0) of (a) wheat bran (WB) control, and WB after 14 days of solid-state fermentation with (b) *F. fomentarius* (FF) (c) *G. lucidum* (GL) and (d) *P. ostreatus* (PO). Structures of annotated correlation peaks are presented in the lower part of the figure. FA: ferulate, SA: sinapates, S: syringyl unit, X: β-D-xylopyranoside, A: α-L-arabinofuranoside. Colors match the assigned contours. Unassigned signals are presented in gray.

carbohydrate linkages in which ferulates participate (Hatfield et al., 2017). Nevertheless, given the substantial reduction in arabinoxylans (Fig. 2a), the specific removal of AX-linked ferulates and diferulates cannot be excluded. Cleavage of these structures is usually facilitated by feruloyl esterases, which *F. fomentarius* efficiently produces extracellularly (Perna et al., 2018).

In the anomeric carbohydrate region, signals for arabinose, xylose, α-glucans (starch), and sucrose, were observed. However, heavy overlap with carbohydrate signals from the fungal mycelium hinder the unambiguous identification of the signals from the substrate. Arabinose (A_1)

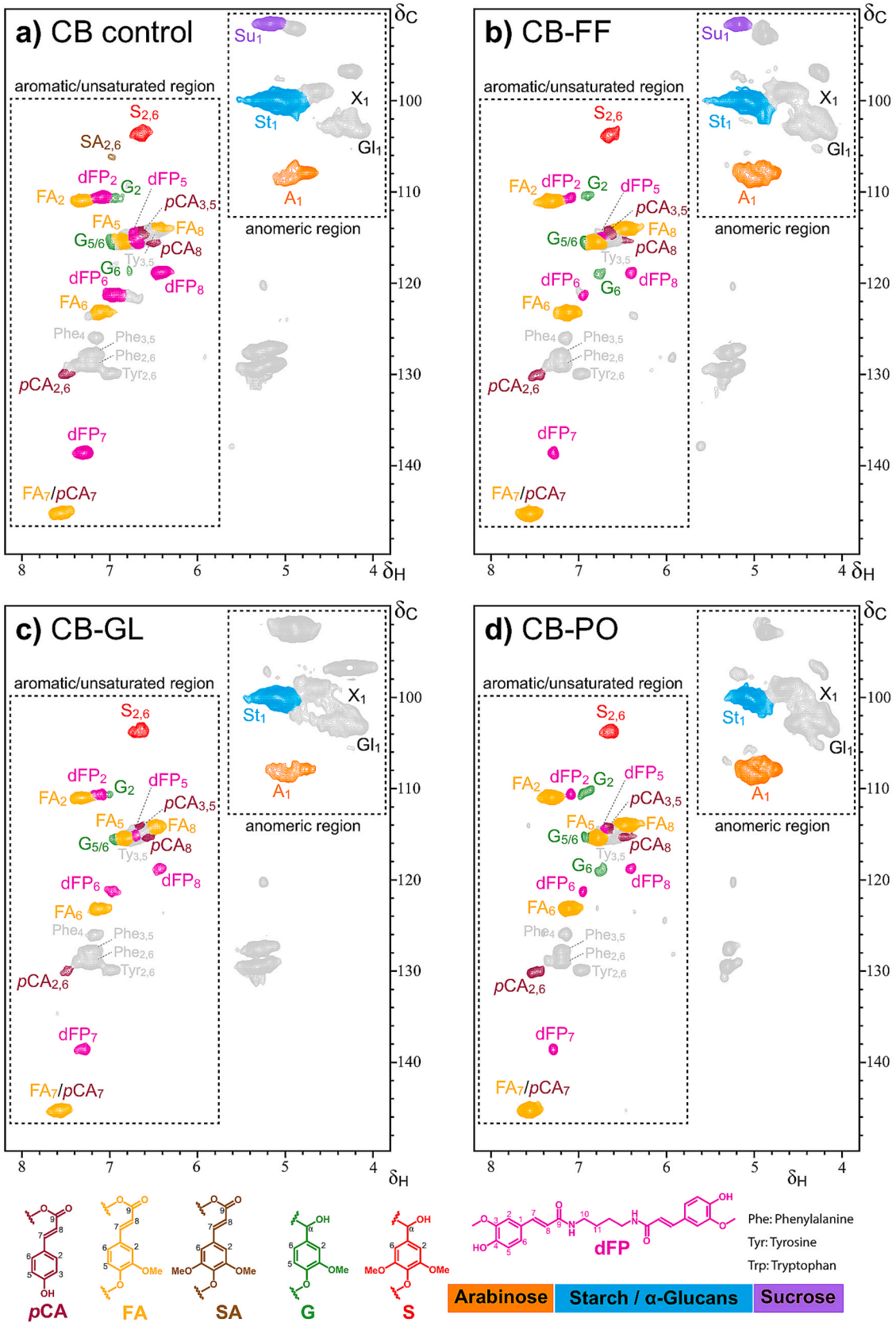

Fig. 5. 2D-HSQC spectra (δ_C/δ_H = 90–150/3.8–8.0) of (a) corn bran (CB) control, and CB after 14 days of fermentation with (b) *F. fomentarius* (FF) (c) *G. lucidum* (GL) and (d) *P. ostreatus* (PO). Structures of annotated correlation peaks are presented in the lower part of the figure. *p*CA: *p*-coumarate, FA: ferulate, SA: sinapates, G: guaiacyl unit, S: syringyl unit, dFP: diferuloylputrescine. Colors match the assigned contours. Unassigned signals are presented in gray.

Table 2
HSQC signal integration values normalized to the residual DMSO signal used as an internal reference (as signals $S_{2,6}$, $SA_{2,6}$, and $pCA_{2,6}$ correspond to two proton-carbon pairs their volume integrals were halved).

	Wheat bran				Corn bran			
Signals	Control	PO	FF	GL	Control	PO	FF	GL
Aromatic/unsaturated								
Lignin S-units ($S_{2,6}$)	6.9	2.7	0.8	2.7	24.6	23.6	21.7	15.3
Lignin G-units (G_2)	2.0	1.5	2.5	2.7	9.6	26.6	20.3	6.7
S/G ratio	3.4	1.8	0.3	1.0	2.4	0.9	1.1	2.3
Sinapates ($SA_{2,6}$)	4.4	tr.	tr.	tr.	4.8	tr.	tr.	tr.
Ferulates (FA_2)	52.6	tr.	tr.	10.2	55.3	199.2	142.8	42.4
p-Coumarates ($pCA_{2,6}$)	n.d.	n.d.	n.d.	n.d.	10.5	17.3	11.5	15.1
Diferuloylputrescine (dFP_7)	n.d.	n.d.	n.d.	n.d.	51.0	17.2	21.8	7.6
Anomeric carbohydrates								
Arabinose (A_1)	175.7	126.9	138.5	111.8	118.9	296.5	207.6	75.0
Starch (St_1)	973.0	80.6	49.1	15.4	1397.6	731.6	1189.3	517.6
Sucrose (Su_1)	602.8	tr.	416.0	193.5	235.7	n.d.	192.1	n.d.

n.d.: not detected.
tr.: trace amounts.

signals slightly decreased across all species, with the most markedly with *G. lucidum*, followed by *P. ostreatus* and *F. fomentarius*. Fermentation preferentially affected $A(X^3)$ and $A(A^5)$ residues, suggesting selective removal of specific arabinoxylan side-chain substitutions. Arabinose is cleaved from the xylan backbone by arabinofuranosidases, enzymes belonging to the glycoside hydrolase class, with di-substituted $A(A^5)$ motifs requiring enzymes with broader selectivity such as those from the GH51 and GH54 families (dos Santos et al., 2018). Similarly, the anomeric α-glucan signal (St_1, starch) also decreased strongly after fermentation, mostly with *G. lucidum*, followed by *F. fomentarius* and *P. ostreatus*. Contribution of fungal biomass to this signal may have underestimated starch degradation, though quantification values in Fig. 2a confirm a similar order of starch removal across species. Sucrose (Su_1) was particularly prominent in WB control, but no longer detectable after fermentation with *P. ostreatus*. *G. lucidum* reduced it substantially, whereas *F. fomentarius* only partially (Table 2).

In contrast, CB displayed a more complex aromatic profile (Fig. 5), with higher lignin content and the presence of clear signals for both S- and G-lignin units. The major aromatic components corresponded to the hydroxycinnamates ferulates (FA), *p*-coumarates (*p*CA), and sinapates (SA), along with diferuloylputrescine (dFP), a ferulic acid amide previously reported to be incorporated into the lignin polymer of corn kernels (del Río et al., 2018).

Overall, *G. lucidum* exhibited the strongest effect on both S- and G-lignin units signals (Table 2), while *F. fomentarius* and *P. ostreatus* had a minimal impact on these structures. Fermentation with *F. fomentarius* and *P. ostreatus* however markedly decreased the lignin S/G ratios indicating preferentially targeting of S-type lignin, as occurred with WB. The apparent increase in G-unit signal intensity likely reflected a relative enrichment due to preferential removal of other cell wall components rather than actual lignin accumulation.

Among hydroxycinnamates, SA was completely removed by all three fungi, while FA and *p*CA signals were only slightly reduced after fermentation with *G. lucidum*. *F. fomentarius* and *P. ostreatus* instead showed an apparent increase in their signal intensities, consistent with the phenolic concentrations determined by HPLC (Fig. 3b). This is more plausibly attributed to a relative enrichment from the degradation of other cell wall components, though the generation of ferulates from precursors such as dFP, reduced by all species to a similar extent (approximately 65%), cannot be excluded. The parallel reduction of ferulate and arabinose anomeric signals upon *G. lucidum* fermentation (Table 2), strongly supports that ferulates in CB were predominantly ester-linked to arabinose rather than in free form, as further evidenced by the absence of the characteristic free ferulic acid signal (FA_8) (Schendel and Bunzel, 2022). Hydroxycinnamates degradation during white-rot fungal fermentation is primarily mediated by laccases, that have been shown to exhibit higher affinity towards more methoxylated substrates, such as sinapic acid (Perna et al., 2018).

As also observed in WB, the anomeric α-glucans signal (St_1, starch) decreased after CB fermentation, most prominently with *G. lucidum*, followed by *P. ostreatus* and, to a lesser extent, *F. fomentarius*, consistent with the analytical results in Fig. 2c. The sucrose signal (Su_1) was similarly reduced, becoming undetectable after fermentation with *P. ostreatus* and *G. lucidum* (Table 2, Fig. 5).

While the compositional analysis quantified the overall changes in the carbohydrate and phenolic fractions, NMR provided additional structural insights into the specific linkages and substructures affected by fungal fermentation. The three fungal species exhibited distinct degradation strategies, which were modulated to varying extents by the substrate. *P. ostreatus* consistently prioritized amorphous carbohydrates, such as starch, over cellulose and phenolics in both substrates. In contrast, *F. fomentarius* demonstrated a more substrate-dependent behavior, extensively degrading carbohydrates, cellulose and phenolic moieties in WB, but showed reduced carbohydrolytic activity in the more recalcitrant CB, where hydroxycinnamates and lignin were relatively enriched. Interestingly, *G. lucidum* was the most selective, preferentially targeting aromatic compounds, particularly in CB, where S- and G- lignin signals reduced markedly. Although *G. lucidum* is considered a simultaneous degrader of holocellulose and lignin (Kainthola et al., 2019), these findings suggest that substrate composition strongly redirect its degradative behavior.

3.5. Fungal enzymatic profiling over SSF

The major enzymes involved in lignocellulose degradation by white-rot fungi, cellulases, xylanases, and laccases, can be regulated depending on the degradation stage (Alfaro et al., 2020). Cellulases and xylanases include mostly a set of glycoside hydrolases that facilitating polysaccharide hydrolysis, while laccases are oxidative enzymes acting on lignin and phenolics (Andlar et al., 2018). In this study, enzyme activities were classified into low, medium and high categories using tertile-based thresholds across all measurements. The heatmaps in Fig. 6a, 6b and 6c display the categorical activity levels.

Wheat bran (WB) supported higher hydrolytic activity than corn bran (CB) across all species, except for xylanases in *P. ostreatus,* which exhibited notable biological variability (Fig. 6a). This is consistent with the lower carbohydrate depletion in CB, suggesting its structural recalcitrance likely suppressed the activity of hydrolases (Andlar et al., 2018). Cellulase activity (*endo*-1,4-β-D-glucanase) remained constant across both substrates in *P. ostreatus* extracts, peaked on days 5 and 7

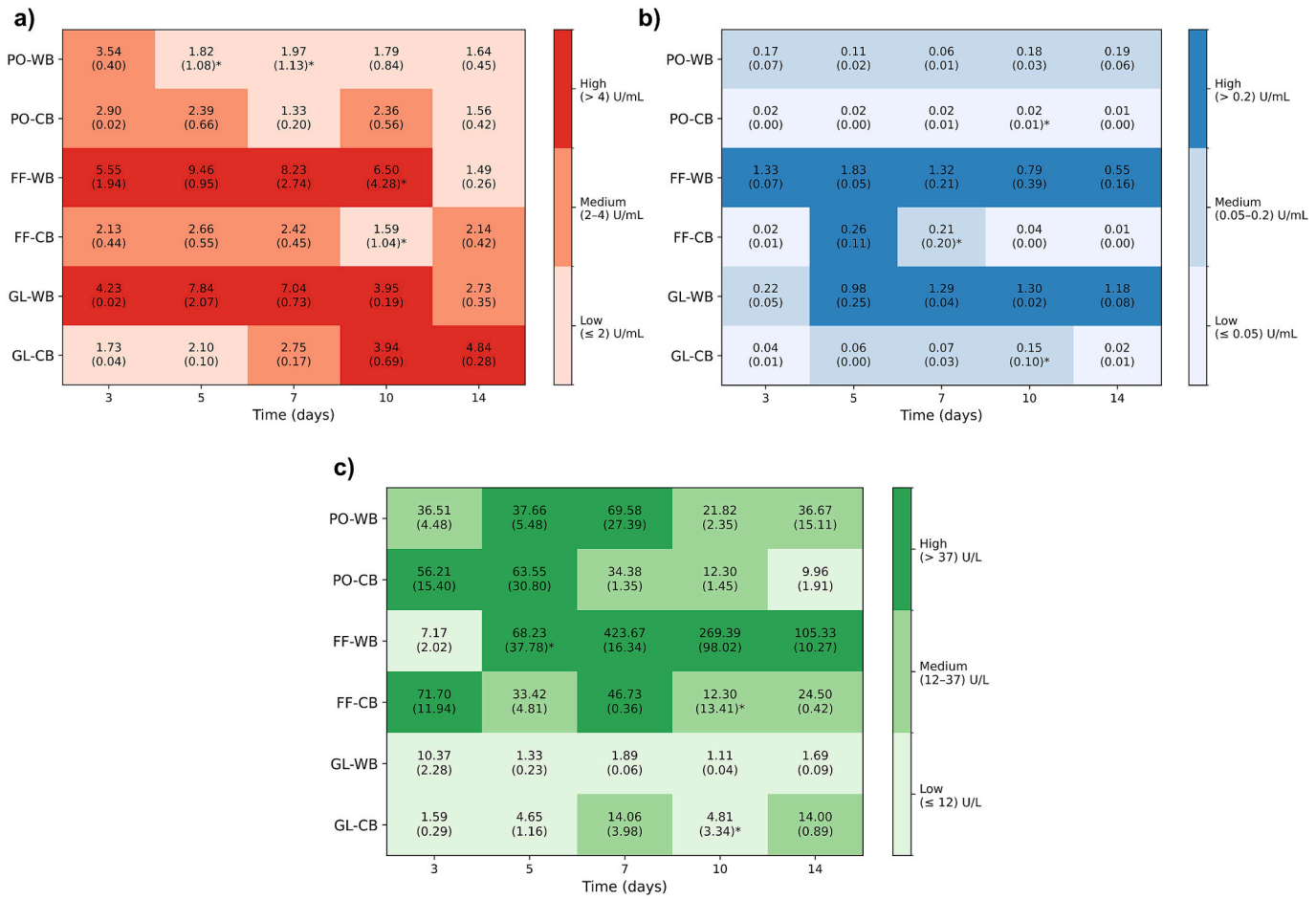

Fig. 6. Discrete heatmaps of enzyme activity of (a) Xylanases (U/mL), (b) Cellulases (*endo*-1,4-β-D-glucanase) (U/mL) and (c) Laccases (U/L) after 3, 5, 7, 10 and 14 days of solid-state fermentation of wheat bran (WB) and corn bran (CB) with *P. ostreatus* (PO), *F. fomentarius* (FF) and *G. lucidum* (GL). Cells with an * indicate conditions where the standard deviation exceeded the 50 % of the mean, highlighting high variability. Values in parenthesis correspond to the standard deviation (n = 3 biological replicates).

before decreasing in *F. fomentarius* grown on CB and remained stable but in higher leveks for *G. lucidum* on WB. It should be noted that cellulase activity, measured on a β-glucan substrate, reflects only *endo*-1,4-β-D-glucanase activity, not total cellulases (β-glucosidase, *exo*-1,4-β-D-glucanase). As xylanases also release hemicellulose-linked phenolics (Andlar et al., 2018), the increased hydrolase activity together with the low activity of laccases during *G. lucidum* fermentation of WB may explain the accumulation of soluble phenolics, as shown in Fig. 3c.

Laccase activity in *P. ostreatus* extracts was higher early in fermentation, likely facilitating carbohydrate accessibility by detoxifying phenolics and partially modifying the lignocellulosic matrix (Giacobbe et al., 2018). This is consistent with the observed reduction in carbohydrates and the 2D-HSQC results (Fig. 2, Fig. 4, Fig. 5). Oxidoreductases dominate *P. ostreatus* secretomes on both woody and non-woody substrates, with only slight overproduction of carbohydrate-active enzymes (Fernández-Fueyo et al., 2016). In contrast, *F. fomentarius* extracts exhibited higher laccase activity towards the end of WB fermentation, that alongside the extensive decrease of polysaccharides (Fig. 2a) suggest a carbohydrate preferential strategy. *G. lucidum* displayed the lowest laccase activity among the species, regardless of substrate or fermentation time.

4. Conclusions

This study demonstrates that fungal degradation strategies during solid-state fermentation depend strongly on substrate and species. Wheat bran supported faster colonization and greater compositional modifications than corn bran, mostly due to its higher content of accessible polysaccharides. All fungi preferentially degraded starch early in fermentation, before proceeding to modifying structural carbohydrates, with rising ergosterol and protein levels reflecting fungal biomass accumulation. *Fomes fomentarius* exhibited the most pronounced depletion of cellulose and arabinoxylans, indicating a carbohydrate targeting strategy. *Pleurotus ostreatus* showed a reduction of phenolic acids in wheat bran together with increased early-stage oxidative activity, while *Ganoderma lucidum* preferentialy mobilized phenolic moieties with limited cellulose depolymerization. By integrating compositional, spectroscopic and enzymatic analysis, this work provides mechanistic insights into species-specific biomass conversion, that can guide the selection of fungal species for targeted cereal bran valorization, including pretreatment for biorefineries, enzyme production, and development of value-added feed and biobased products.

CRediT authorship contribution statement

Chloe Rantzos: Writing – review & editing, Writing – original draft, Visualization, Validation, Methodology, Investigation, Formal analysis, Data curation, Conceptualization. **Jorge Rencoret:** Writing – review & editing, Writing – original draft, Visualization, Validation, Methodology, Investigation, Formal analysis. **José C. del Río:** Writing – review & editing, Writing – original draft, Visualization, Validation, Methodology, Investigation, Formal analysis. **Amparo Jiménez-Quero:** Writing –

review & editing, Writing – original draft, Validation, Supervision, Resources, Project administration, Methodology, Investigation, Funding acquisition, Conceptualization.

Declaration of competing interest

The authors declare that they have no known competing financial interests or personal relationships that could have appeared to influence the work reported in this paper.

Acknowledgments

CR and AJQ acknowledge funding from the Knut and Alice Wallenberg Foundation (KAW) through the Wallenberg Wood Science Center, WWSC 3.0: KAW 2021.0313 and from the Swedish Research Council Formas (Project MYCOMYM 2022-00401). JR and JCdR were supported by project PID2023-152543OB-I00, funded by the Spanish MICIU/AEI/10.13039/501100011033 and the European Regional Development Fund (ERDF) "A way of making Europe".

Appendix A. Supplementary data

Supplementary data to this article can be found online at https://doi.org/10.1016/j.biortech.2026.135424.

Data availability

Data will be made available on request.

References

Akbari, M., Razavi, S.H., Khodaiyan, F., Blesa, J., Esteve, M.J., 2023. Fermented corn bran: a by-product with improved total phenolic content and antioxidant activity. LWT 184, 115090. https://doi.org/10.1016/j.lwt.2023.115090.

Alfaro, M., Majcherczyk, A., Kües, U., Ramírez, L., Pisabarro, A.G., 2020. Glucose counteracts wood-dependent induction of lignocellulolytic enzyme secretion in monokaryon and dikaryon submerged cultures of the white-rot basidiomycete *Pleurotus ostreatus*. Sci. Rep. 10, 12421. https://doi.org/10.1038/s41598-020-68969-1.

Andlar, M., Rezić, T., Marđetko, N., Kracher, D., Ludwig, R., Šantek, B., 2018. Lignocellulose degradation: an overview of fungi and fungal enzymes involved in lignocellulose degradation. Eng. Life Sci. 18, 768–778. https://doi.org/10.1002/elsc.201800039.

Bailey, M.J., Biely, P., Poutanen, K., 1992. Interlaboratory testing of methods for assay of xylanase activity. J. Biotechnol. 23, 257–270. https://doi.org/10.1016/0168-1656(92)90074-j.

Castaño, J.D., Muñoz-Muñoz, N., Kim, Y.M., Liu, J., Yang, L., Schilling, J.S., 2022. Metabolomics highlights different life history strategies of white and brown rot wood-degrading fungi. mSphere 7. https://doi.org/10.1128/msphere.00545-22.

Castorina, G., Cappa, C., Negrini, N., Criscuoli, F., Casiraghi, M.C., Marti, A., Rollini, M., Consonni, G., Erba, D., 2023. Characterization and nutritional valorization of agricultural waste corncobs from italian maize landraces through the growth of medicinal mushrooms. Sci. Rep. 13, 21148. https://doi.org/10.1038/s41598-023-48252-9.

Cazier, E.A., Pham, T.N., Cossus, L., Abla, M., Ilc, T., Lawrence, P., 2024. Exploring industrial lignocellulosic waste: sources, types, and potential as high-value molecules. Waste Manag. 188, 11–38. https://doi.org/10.1016/j.wasman.2024.07.029.

Cicco, N., Lanorte, M.T., Paraggio, M., Viggiano, M., Lattanzio, V., 2009. A reproducible, rapid and inexpensive Folin–Ciocalteu micro-method in determining phenolics of plant methanol extracts. Microchem. J. 91, 107–110. https://doi.org/10.1016/j.microc.2008.08.011.

del Río, J.C., Rencoret, J., Gutiérrez, A., Kim, H., Ralph, J., 2018. Structural characterization of lignin from maize (*Zea mays* L.) fibers: evidences for diferuloylputrescine incorporated into the lignin polymer in maize kernels. J. Agric. Food Chem. 66, 4402–4413. https://doi.org/10.1021/acs.jafc.8b00880.

dos Santos, C.R., De Giuseppe, P.O., De Souza, F.H.M., Zanphorlin, L.M., Domingues, M. N., Pirolla, R.A.S., Honorato, R.V., Tonoli, C.C.C., De Morais, M.A.B., De Matos Martins, V.P., Fonseca, L.M., Büchli, F., De Oliveira, P.S.L., Gozzo, F.C., Murakami, M.T., 2018. The mechanism by which a distinguishing arabinofuranosidase can cope with internal di-substitutions in arabinoxylans. Biotechnol. Biofuels 11, 223. https://doi.org/10.1186/s13068-018-1212-y.

Fernández-Fueyo, E., Ruiz-Dueñas, F.J., López-Lucendo, M.F., Pérez-Boada, M., Rencoret, J., Gutiérrez, A., Pisabarro, A.G., Ramírez, L., Martínez, A.T., 2016. A secretomic view of woody and nonwoody lignocellulose degradation by *Pleurotus ostreatus*. Biotechnol. Biofuels 9, 49. https://doi.org/10.1186/s13068-016-0462-9.

Gari, M.T., Asfaw, B.T., Abo, L.D., Jayakumar, M., Kefalew, G., 2024. Effective utilization of agricultural cereal grains in value-added products: A global perspective. In: Cherian, E., Gurunathan, B. (Eds.), Value Added Products From Food Waste. Springer, pp. 41–58. https://doi.org/10.1007/978-3-031-48143-7_3.

Giacobbe, S., Pezzella, C., Lettera, V., Sannia, G., Piscitelli, A., 2018. Laccase pretreatment for agrofood wastes valorization. Bioresour. Technol. 265, 59–65. https://doi.org/10.1016/j.biortech.2018.05.108.

Gonçalves, C., Rodriguez-Jasso, R.M., Gomes, N., Teixeira, J.A., Belo, I., 2010. Adaptation of dinitrosalicylic acid method to microtiter plates. Anal. Methods 2, 2046–2048. https://doi.org/10.1039/c0ay00525h.

Goudopoulou, A., Krimitzas, A., Typas, M.A., 2010. Differential gene expression of ligninolytic enzymes in *Pleurotus ostreatus* grown on olive oil mill wastewater. Appl. Microbiol. Biotechnol. 88, 541–551. https://doi.org/10.1007/s00253-010-2750-9.

Gow, N.A.R., Latge, J.-P., Munro, C.A., 2017. The Fungal Cell Wall: Structure, Biosynthesis, and Function. Microbiol. Spectr. 5. https://doi.org/10.1128/microbiolspec.funk-0035-2016.

Hadidi, M., Garcia, S.R., Ziogkas, D., McClements, D.J., Moreno, A., 2024. Cereal bran proteins: recent advances in extraction, properties, and applications. Crit. Rev. Food Sci. Nutr. 64, 10583–10607. https://doi.org/10.1080/10408398.2023.2226730.

Hatfield, R.D., Rancour, D.M., Marita, J.M., 2017. Grass cell walls: a story of cross-linking. Front. Plant Sci. 7, 204954. https://doi.org/10.3389/fpls.2016.02056.

Heidari, F., Øverland, M., Hansen, J.Ø., Mydland, L.T., Urriola, P.E., Chen, C., Shurson, G.C., Hu, B., 2022. Solid-state fermentation of *Pleurotus ostreatus* to improve the nutritional profile of mechanically-fractionated canola meal. Biochem. Eng. J. 187, 108591. https://doi.org/10.1016/j.bej.2022.108591.

Kähkönen, M.P., Hopia, A.I., Vuorela, H.J., Rauha, J.P., Pihlaja, K., Kujala, T.S., Heinonen, M., 1999. Antioxidant activity of plant extracts containing phenolic compounds. J. Agric. Food Chem. 47, 3954–3962. https://doi.org/10.1021/jf9901461.

Kainthola, J., Kalamdhad, A.S., Goud, V.V., Goel, R., 2019. Fungal pretreatment and associated kinetics of rice straw hydrolysis to accelerate methane yield from anaerobic digestion. Bioresour. Technol. 286, 121368. https://doi.org/10.1016/j.biortech.2019.121368.

Kim, H., Padmakshan, D., Li, Y., Rencoret, J., Hatfield, R.D., Ralph, J., 2017. Characterization and elimination of undesirable protein residues in plant cell wall materials for enhancing lignin analysis by solution-state nuclear magnetic resonance spectroscopy. Biomacromolecules 18, 4184–4195. https://doi.org/10.1021/acs.biomac.7b01223.

Kim, H., Ralph, J., Akiyama, T., 2008. Solution-state 2D NMR of ball-milled plant cell wall gels in DMSO-d_6. Bioenergy Res. 1, 56–66. https://doi.org/10.1007/s12155-008-9004-z.

Mäkelä, M.R., Marinović, M., Nousiainen, P., Liwanag, A.J.M., Benoit, I., Sipilä, J., Hatakka, A., de Vries, R.P., Hildén, K.S., 2015. Aromatic metabolism of filamentous fungi in relation to the presence of aromatic compounds in plant biomass. Adv. Appl. Microbiol. 91, 63–137. https://doi.org/10.1016/bs.aambs.2014.12.001.

Martínez, A. T., Speranza, M., Ruiz-Dueñas, F. J., Ferrera, P., Camarero, S., Martínez, M. J., Gutiérrez, A., del Río, J. C., 2005. Biodegradation of lignocellulosics: microbiological, chemical and enzymatic aspects of fungal attack to lignin. Int. Microbiol. 8, 195–204. (PubMed ID: 16200498).

Medina-Remón, A., Barrionuevo-González, A., Zamora-Ros, R., Andres-Lacueva, C., Estruch, R., Martínez-González, M.Á., Diez-Espino, J., Lamuela-Raventos, R.M., 2009. Rapid Folin–Ciocalteu method using microtiter 96-well plate cartridges for solid phase extraction to assess urinary total phenolic compounds, as a biomarker of total polyphenols intake. Anal. Chim. Acta 634, 54–60. https://doi.org/10.1016/j.aca.2008.12.012.

Mnich, E., Bjarnholt, N., Eudes, A., Harholt, J., Holland, C., Jørgensen, B., Larsen, F.H., Liu, M., Manat, R., Meyer, A.S., Mikkelsen, J.D., Motawia, M.S., Muschiol, J., Møller, B.L., Møller, S.R., Perzon, A., Petersen, B.L., Ravn, J.L., Ulvskov, P., 2020. Phenolic cross-links: building and de-constructing the plant cell wall. Nat. Prod. Rep. 37, 919–961. https://doi.org/10.1039/c9np00028c.

More, S.S., Renuka, P.S., Pruthvi, K., Swetha, M., Malini, S., Veena, S.M., 2011. Isolation, purification, and characterization of fungal laccase from Pleurotus sp. Enzyme Res. 2011, 248735. https://doi.org/10.4061/2011/248735.

Nejati, M., Zha, L., Mensah, R.A., Das, O., Capezza, A.J., Jiménez-Quero, A., 2026. Agro-food waste upcycling into mycelium insulation: linking structure with mechanical and fire performance. Mater. Today Sustain. 33, 101295. https://doi.org/10.1016/j.mtsust.2025.101295.

Pasanen, A.L., Yli-Pietilä, K., Pasanen, P., Kalliokoski, P., Tarhanen, J., 1999. Ergosterol content in various fungal species and biocontaminated building materials. Appl. Environ. Microbiol. 65, 138–142. https://doi.org/10.1128/aem.65.1.138-142.1999.

Pereira, P.F., Jiménez-Quero, A., 2025. Circular valorization of green leafy side streams via pressurized liquid extraction techniques for recovery of bioactive compounds. Food Chem. X, 102944. https://doi.org/10.1016/j.fochx.2025.102944.

Perna, V., Agger, J.W., Holck, J., Meyer, A.S., 2018. Multiple reaction monitoring for quantitative laccase kinetics by LC-MS. Sci. Rep. 8, 8114. https://doi.org/10.1038/s41598-018-26523-0.

Qazanfarzadeh, Z., de Moura, F., Pereira, P., Jiménez-Quero, A., 2026. Fungal Polysaccharides. Purification and Characterization 43–55. https://doi.org/10.1007/978-1-0716-4989-3_3.

Rencoret, J., Marques, G., Gutiérrez, A., Nieto, L., Santos, J.I., Jiménez-Barbero, J., Martínez, Á.T., del Río, J.C., 2009. HSQC-NMR Analysis of lignin in woody (*Eucalyptus globulus* and *Picea abies*) and non-woody (*Agave sisalana*) ball-milled plant materials at the gel state. Holzforschung 63, 691–698. https://doi.org/10.1515/hf.2009.070.

Roye, C., Bulckaen, K., De Bondt, Y., Liberloo, I., Van De Walle, D., Dewettinck, K., Courtin, C.M., 2020. Side-by-side comparison of composition and structural

properties of wheat, rye, oat, and maize bran and their impact on in vitro fermentability. Cereal Chem. 97, 20–33. https://doi.org/10.1002/cche.10213.
Rubio-Ríos, J., Pérez, J., Salinas, M.J., Fenoy, E., López-Rojo, N., Boyero, L., Casas, J.J., 2021. Key plant species and detritivores drive diversity effects on instream leaf litter decomposition more than functional diversity: a microcosm study. Sci. Tot. Environ. 798, 149266. https://doi.org/10.1016/j.scitotenv.2021.149266.
Ruthes, A.C., Rudjito, R.C., Rencoret, J., Gutiérrez, A., Del Río, J.C., Jiménez-Quero, A., Vilaplana, F., 2020. Comparative recalcitrance and extractability of cell wall polysaccharides from cereal (wheat, rye, and barley) brans using subcritical water. ACS Sustain. Chem. Eng. 8, 7192–7204. https://doi.org/10.1021/acssuschemeng.0c01764.
Saharan, P., Sadh, P.K., Singh Duhan, J., 2017. Comparative assessment of effect of fermentation on phenolics, flavanoids and free radical scavenging activity of commonly used cereals. Biocatal. Agric. Biotechnol. 12, 236–240. https://doi.org/10.1016/j.bcab.2017.10.013.
Schendel, R.R., Bunzel, M., 2022. 2D-HSQC-NMR-based screening of feruloylated side-chains of cereal grain arabinoxylans. Front. Plant Sci. 13, 951705. https://doi.org/10.3389/fpls.2022.951705.
Šelo, G., Planinić, M., Tišma, M., Klarić, A.M., Bucić-Kojić, A., 2024. Effects of fungal solid-state fermentation on the profile of phenolic compounds and on the nutritional properties of grape pomace. Microorganisms 12, 1310. https://doi.org/10.3390/microorganisms12071310.
Shankar, A., Saini, S., Sharma, K.K., 2022. Fungal-integrated second-generation lignocellulosic biorefinery: utilization of agricultural biomass for co-production of lignocellulolytic enzymes, mushroom, fungal polysaccharides, and bioethanol. Biomass Convers. Biorefin. 14, 1117–1131. https://doi.org/10.1007/S13399-022-02969-1.
Sharma, G., Kumar, M., Pandey, A.K., Kumari, S., Singh, A., Ansari, N.A., Gaur, N.A., 2025. Pretreatment technologies for valorisation of lignocellulosic biomass towards sustainable biorefineries: Comprehensive insights and advances. Bioresour. Technol. Rep. 32, 102336. https://doi.org/10.1016/j.biteb.2025.102336.
Sharma, H.K., Xu, C., Qin, W., 2019. Biological pretreatment of lignocellulosic biomass for biofuels and bioproducts: an overview. Waste Biomass Valoriz. 10, 235–251. https://doi.org/10.1007/s12649-017-0059-y.
Smiderle, F.R., Sassaki, G.L., Van Arkel, J., Iacomini, M., Wichers, H.J., Van Griensven, L. J.L.D., 2010. High molecular weight glucan of the culinary medicinal mushroom Agaricus bisporus is an α-glucan that forms complexes with low molecular weight galactan. Molecules 15, 5818–5830. https://doi.org/10.3390/molecules15085818.
van Erven, G., Nayan, N., Sonnenberg, A.S.M., Hendriks, W.H., Cone, J.W., Kabel, M.A., 2018. Mechanistic insight in the selective delignification of wheat straw by three white-rot fungal species through quantitative 13C-IS py-GC–MS and whole cell wall HSQC NMR. Biotechnol. Biofuels 11, 262. https://doi.org/10.1186/s13068-018-1259-9.
Van Eylen, D., van Dongen, F., Kabel, M., de Bont, J., 2011. Corn fiber, cobs and stover: Enzyme-aided saccharification and co-fermentation after dilute acid pretreatment. Bioresour. Technol. 102, 5995–6004. https://doi.org/10.1016/j.biortech.2011.02.049.
Wei, Y., Xue, J., Shi, J., Li, T., Yuan, H., 2024. Comparative transcriptome analysis explores the mechanism of angiosperm and gymnosperm deadwood degradation by *Fomes fomentarius*. J. Fungi 10, 196. https://doi.org/10.3390/jof10030196.
Weng, M., Cheng, J., Lei, T., Lai, P., Wang, H., Tang, X., Zhang, D., Pan, Y., 2025. Solid-state fermentation with Ganoderma lucidum improves nutritional quality and processing characteristics of wheat (Triticum aestivum L.). LWT 217, 117437. https://doi.org/10.1016/j.lwt.2025.117437.
Wu, N., Tian, F., Moodley, O., Song, B., Jia, C., Ye, J., Lv, R., Qin, Z., Li, C., 2019. Optimization of agro-residues as substrates for Pleurotus pulmonarius production. AMB Express 9, 1–9. https://doi.org/10.1186/s13568-019-0907-1.